Supporting Information

Elucidating the Reversible and Irreversible Self-assembly Mechanisms of Low-Complexity Aromatic-Rich Kinked Peptides and Steric Zipper Peptides

Zenghui Lao[‡a], Yiming Tang[‡a], Xuewei Dong[b], Yuan Tan[a], Xuhua Li[c], Xianshi Liu[a], Le Li[a], Cong Guo*[d], and Guanghong Wei*[a]

a. Department of Physics, State Key Laboratory of Surface Physics, Key Laboratory for Computational Physical Sciences (Ministry of Education), Fudan University, Shanghai, China.
E-mail: ghwei@fudan.edu.cn
b. Center for Soft Condensed Matter Physics and Interdisciplinary Research & School of Physical Science and Technology, Soochow University, Suzhou 215006, Jiangsu, China
c. MOE Key Laboratory for Nonequilibrium Synthesis and Modulation of Condensed Matter, School of Physics, Xi'an Jiaotong University, Xi'an 710049, China.
d. Department of Physics and International Centre for Quantum and Molecular Structures, College of Sciences, Shanghai University, Shanghai, China.
E-mail: congguo@shu.edu.cn

There are 13 supplementary figures.

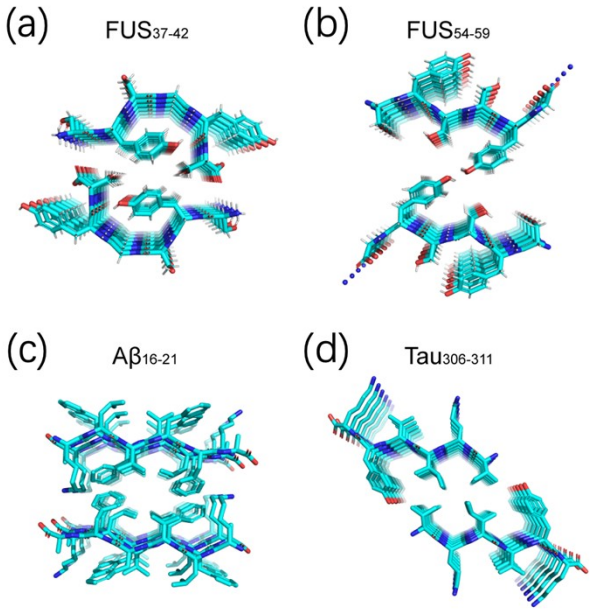

Figure S1. Initial atomic structures of (a) FUS_{37-42} (PDB ID: 5XSG), (b) FUS_{54-59} (PDB ID: 5XRR), (c) $A\beta_{16-21}$ (PDB ID: 3OW9) and (d) $Tau_{306-311}$ (PDB ID: 2ON9) fibrils.

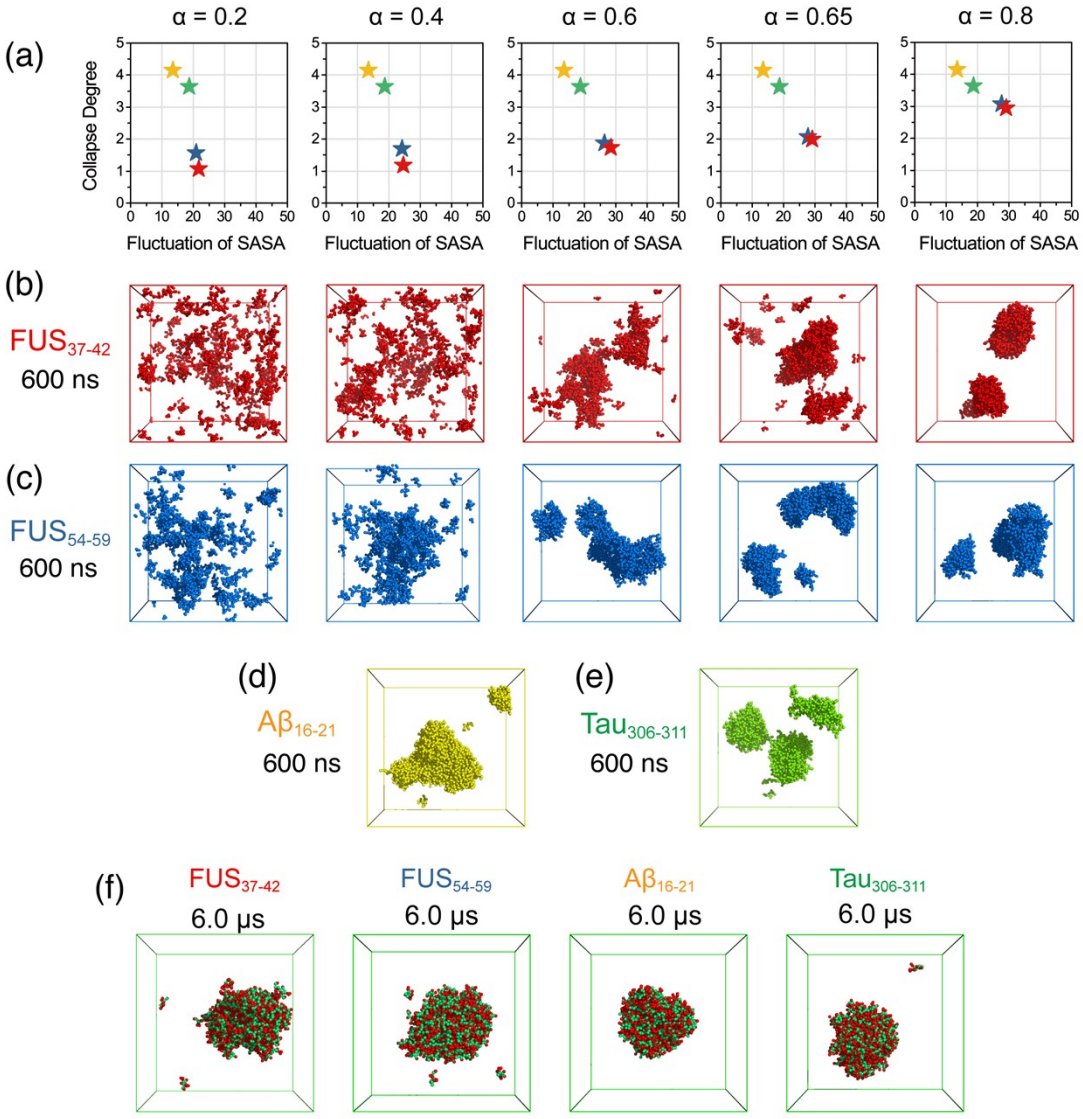

Figure S2. (a) collapse degree and fluctuation of SASA of $FUS_{37–42}$, $FUS_{54–59}$, $A\beta_{16–21}$ and $Tau_{306–311}$ coarse-grained oligomer systems using α values of 0.2, 0.4, 0.6, 0.65 and 0.8. Results are from a 600-ns long CG-MD simulation for each system. (b-c) The final snapshots of the simulations at different α values for (b) $FUS_{37–42}$ and (c) $FUS_{54–59}$ peptide systems. (d-e) The final snapshots of the simulations for $A\beta_{16–21}$ and $Tau_{306–311}$ systems from 600-ns long CG-MD simulations. (f) The final snapshots of the four systems from 6.0-μs-long simulations are shown for comparison.

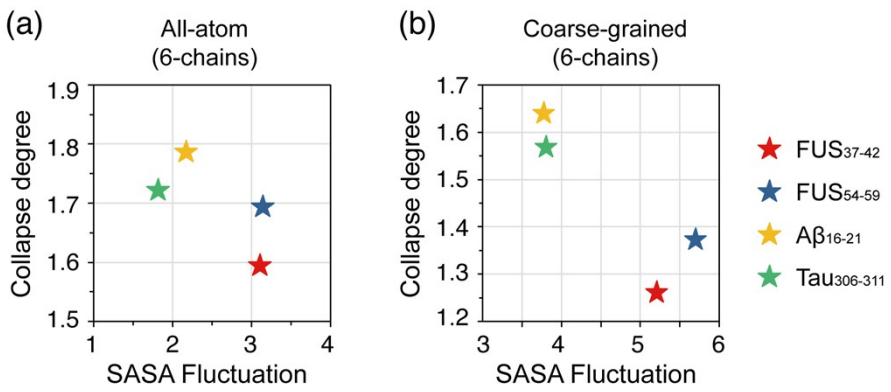

Figure S3. The collapse degree and SASA fluctuation parameters of the four peptides predicted by (a) all-atom and (b) coarse-grained simulations starting from 6 randomly dispersed peptide chains.

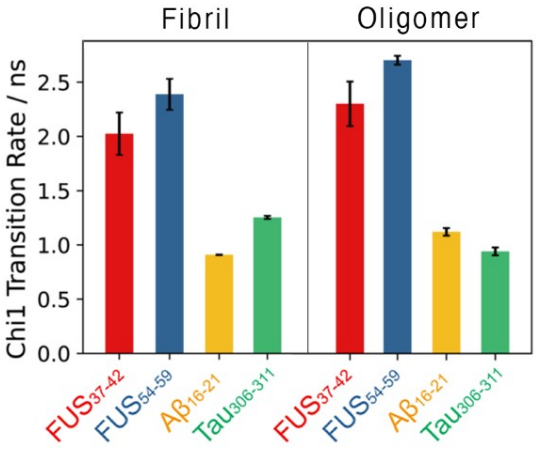

Figure S4. The rate of sidechain dihedral angle (χ_1) transition between the C^{γ}–exo and C^{γ}–endo conformations in the fibril and oligomer systems.

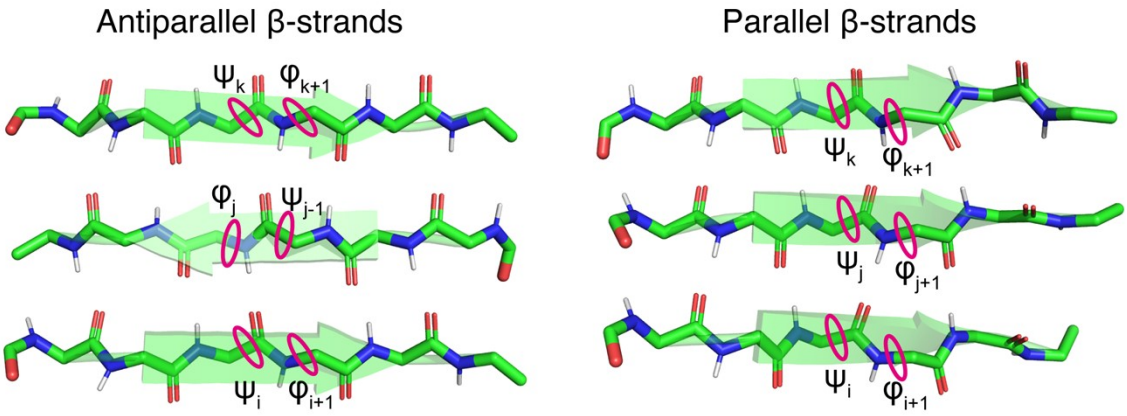

Figure S5. The definitions of the dihedral angles for parallel and antiparallel β-strands.

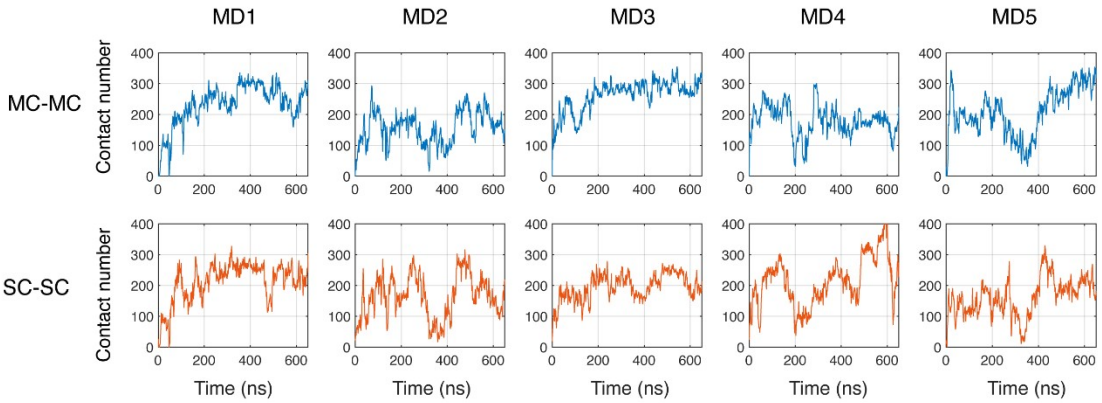

Figure S6. Time evolution of mainchain-mainchain (MC-MC) and sidechain-sidechain (SC-SC) contacts in the five individual simulations for the $A\beta_{16-21}$ systems.

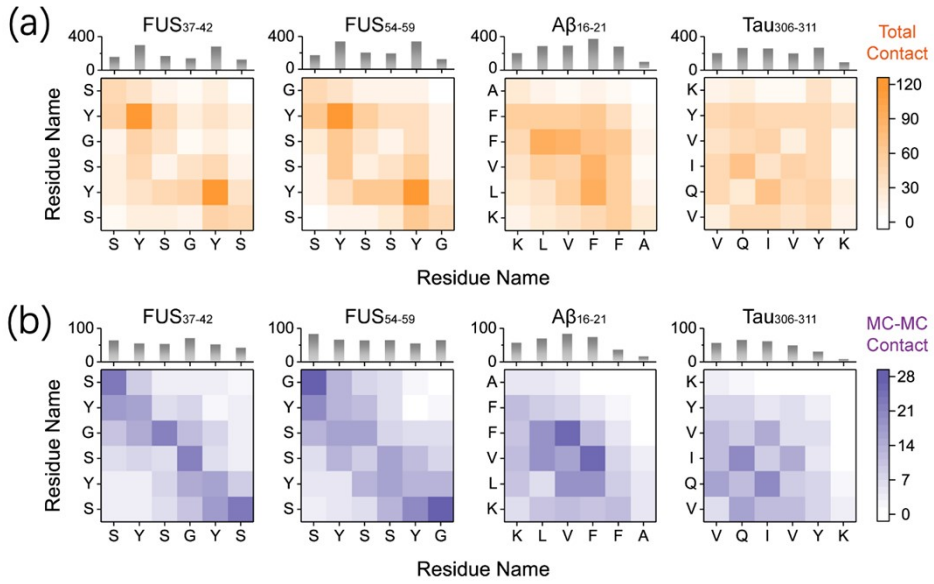

Figure S7. Intermolecular residue-wise (a) total contacts and (b) MC-MC contacts of the four systems. The grey bar charts show the cumulative contact numbers between each residue and other residues.

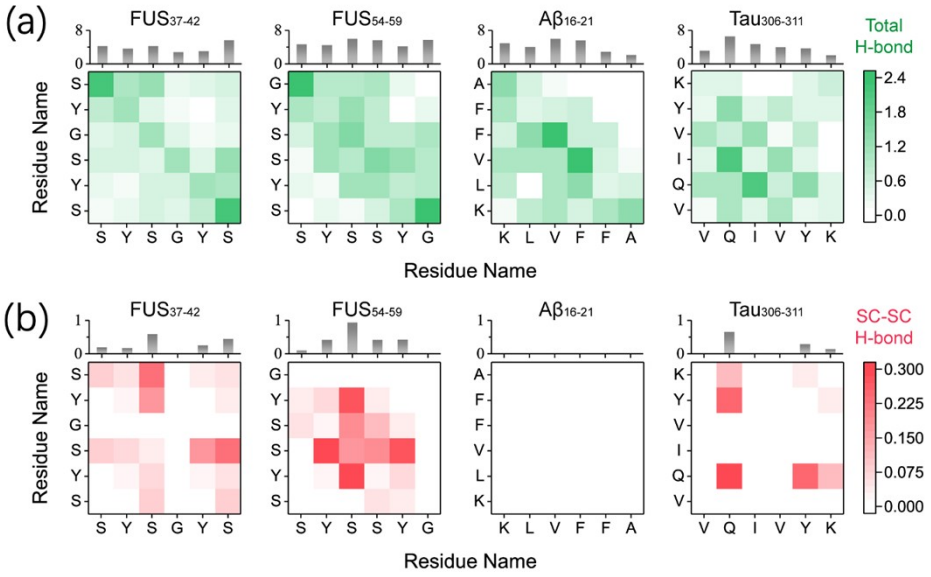

Figure S8. Intermolecular residue-wise (a) total H-bonds and (b) SC-SC H-bonds of the four systems. The grey bar charts show the cumulative H-bond numbers between each residue and other residues.

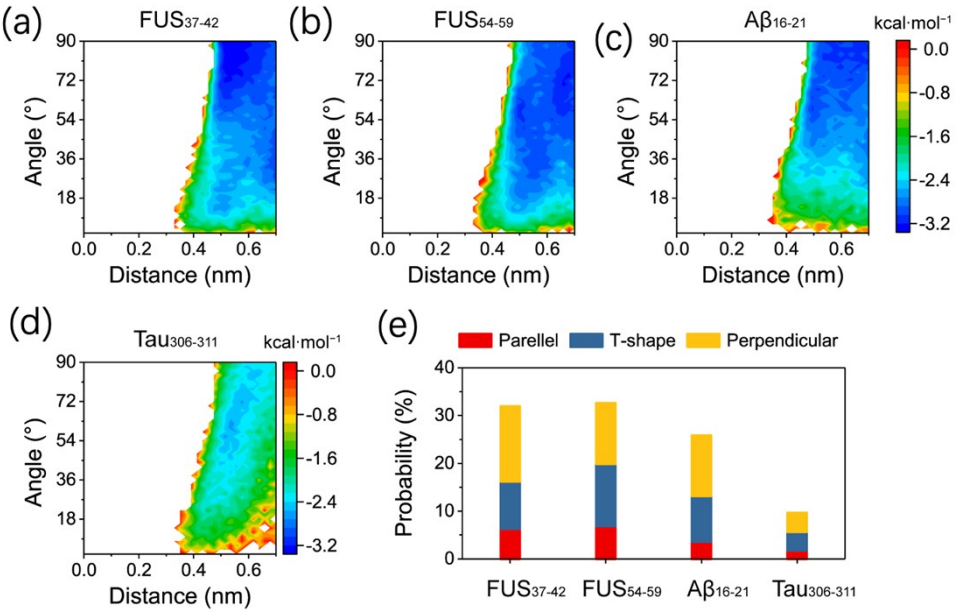

Figure S9. Intermolecular π-π stacking in (A) FUS_{37-42}, (B) FUS_{54-59}, (C) $A\beta_{16-21}$ and (D) $Tau_{306-311}$ all-atom oligomer systems. (E) Probabilities of different patterns of π-π stacking in the four systems.

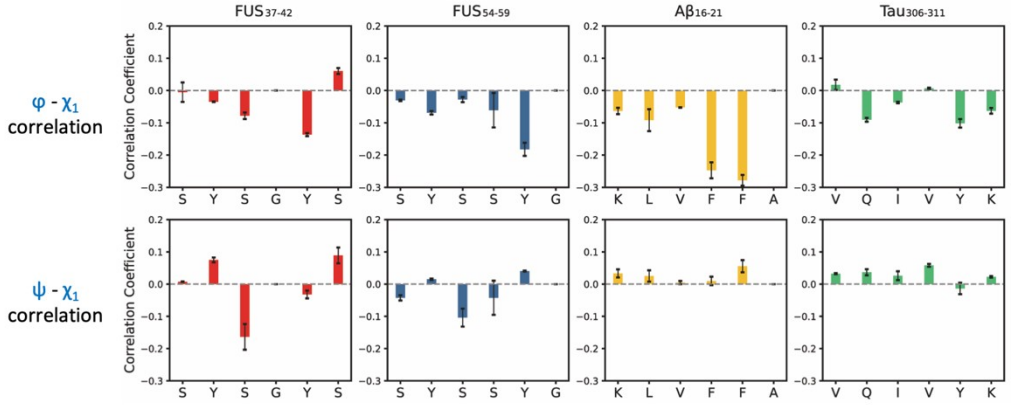

Figure S10. The averaged correlation coefficients between ϕ and χ_1, and those between ψ and χ_1 for each amino acid in the four fibril systems.

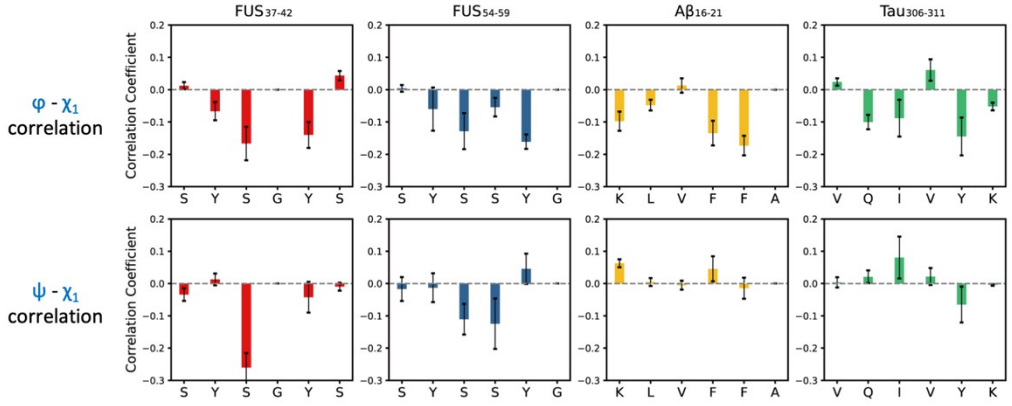

Figure S11. The averaged correlation coefficients between ϕ and χ_1, and those between ψ and χ_1 for each amino acid in the four oligomer systems.

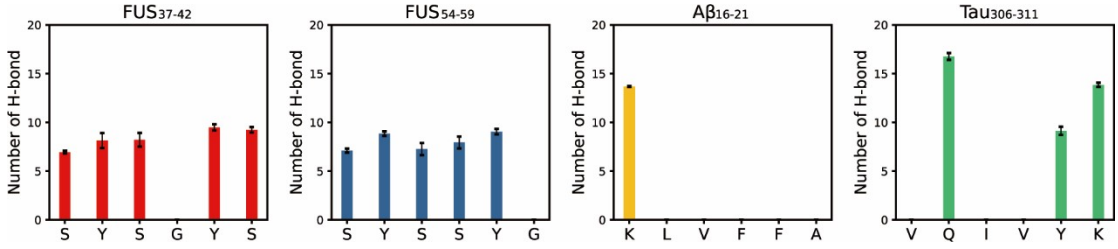

Figure S12. Number of H-bond between sidechain of each residue and water molecules in the four oligomer systems.

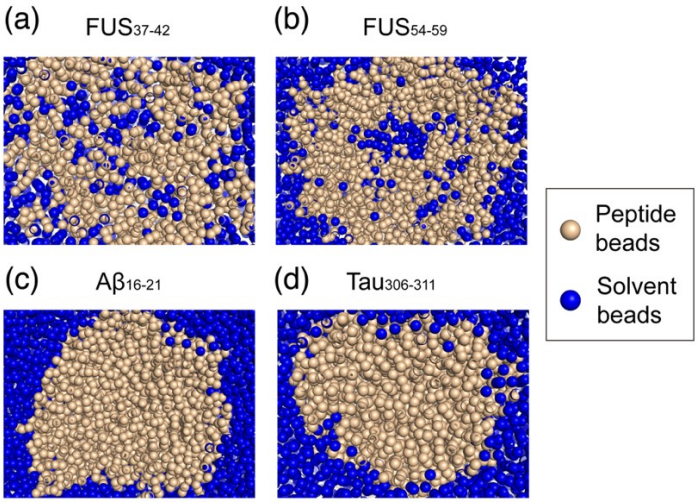

Figure S13. The cross-sections of the aggregates formed by the four peptides showing the contribution of water molecules in the assembly of these peptides.